OXYGEN DELIVERY FROM RED CELLS

ALFRED CLARK, JR.
Department of Mechanical Engineering, University of Rochester, Rochester, New York 14627

WILLIAM J. FEDERSPIEL
Department of Chemical Engineering, University of Rochester, Rochester, New York 14627

PATRICIA A. A. CLARK
Department of Mathematics, Rochester Institute of Technology, Rochester, New York 14623

GILES R. COKELET
Department of Radiation Biology and Biophysics, University of Rochester, Rochester, New York 14642

ABSTRACT This paper deals with the theoretical analysis of the unloading of oxygen from a red cell. A scale analysis of the governing transport equations shows that the solutions have a boundary layer structure near the red-cell membrane. The boundary layer is a region of chemical nonequilibrium, and it owes its existence to the fact that the kinetic time scales are shorter than the diffusion time scales in the red cell. The presence of the boundary layer allows an analytical solution to be obtained by the method of matched asymptotic expansions. A very useful result from the analysis is a simple, lumped-parameter description of the oxygen delivery from a red cell. The accuracy of the lumped-parameter description has been verified by comparing its predictions with results obtained by numerical integration of the full equations for a one-dimensional slab. As an application, we calculate minimum oxygen unloading times for red cells.

INTRODUCTION

A fundamental process in the supply of oxygen to tissue is the unloading of oxygen from a red cell in a capillary. As Hellums (1977) has shown, the internal resistance of the red cell to oxygen transport is not negligible. It is useful to model the unloading process mathematically, so that one can determine the size of this resistance and its dependence on the various parameters of the problem. The unloading process is governed by a pair of diffusion equations, coupled by nonlinear kinetics. In the scaled equations, there are small dimensionless coefficients multiplying the highest spatial derivatives, and the solutions of the equations exhibit boundary layers. These boundary layers make numerical work difficult because they require a fine grid for their resolution. As a result, the previous numerical work, although providing considerable insight, has been limited to one-dimensional slab or cylindrical models (Moll, 1969; Kutchai, 1970; Sheth, 1979; Sheth and Hellums, 1980; Baxley and Hellums, 1983; and Federspiel, 1983).

The very boundary layers that make numerical work difficult, however, provide an opportunity to solve the problem asymptotically. In this paper, we use boundary layer analysis (the method of matched asymptotic expansions) to solve the oxygen unloading problem. The use of the boundary layer concept in the analysis of oxygen transport is not new. It has appeared in steady state, one-dimensional analyses by Keller and Friedlander (1966), Kreuzer and Hoofd (1970, 1972), Gijsbers and Van Ouwerkerk (1976) and others. What is new in the present work is (*a*) the use of the boundary layer theory for the time-dependent, three-dimensional case, and (*b*) the conceptual and mathematical simplicity of the final results.

GLOSSARY

Principal Symbols and Parameter Values

Concentrations	
N_O	oxygen density
N_{Hb}	heme density
N_{HbO}	oxy-heme density
$N_T = N_{Hb} + N_{HbO}$	total heme density (2.03×10^{-5} mol/cm^3)
$S = N_{HbO}/N_T$	fraction saturation
N_{50}	N_O at equilibrium at 50% saturation (4.12×10^{-8} mol/cm^3)
C	N_O/N_{50}, dimensionless oxygen concentration.
Kinetic Constants	
B_U	Bunson coefficient for oxygen (1.56×10^{-9} mol/mmHg/cm^3)
$P_{50} = N_{50}/B_U$	26.4 mmHg
n	dimensionless exponent in Hill equation (2.65)
k	dissociation rate constant (44 s^{-1}).

Dr. W. J. Federspiel's present address is the Department of Biomedical Engineering, Johns Hopkins University, Baltimore, MD 21205.

Diffusion Coefficients

D_O	oxygen diffusion coefficient (9.5×10^{-6} cm^2/s)
$D_{Hb} = D_{HbO}$	heme diffusion coefficients (1.44×10^{-7} cm^2/s).

Length Scales

a	scale of cell half-width (typically 1 μm)
L	cell volume/cell area (0.696 μm).

Times and Time Scales

t	dimensional time
$\tau_{KS} = k^{-1}$	kinetic off time (22.7 ms)
$\tau_{KC} = N_{50}/kN_T$	kinetic on time (46.1 μs)
$\tau_{DS} = a^2/D_{Hb}$	heme diffusion time (69.4 ms for $a = 1$ μm)
$\tau_{DC} = a^2/D_O$	oxygen diffusion time (1.05 ms for $a = 1$ μm)
$\tau_U = (\tau_{DC}/\tau_{KC})^{1/2}\,\tau_{KS}$	unloading time scale (0.108 s for $a = 1$ μm)
$\tau = t/\tau_U$	dimensionless time
t_U	τ_U for $a = L$ (0.0756 s).

BASIC EQUATIONS

Kinetics

For our purposes, the chemical composition at any point in the interior of a red cell is specified by the molar densities of hemoglobins of various degrees of saturation. A complete description of the kinetics would require something like the four-step Adair reaction scheme. The resulting mathematical complexity is hard to justify, however, since the reaction rates for the four steps are not well known. Because of this, we choose the simpler one-step approximation used by many previous authors. Then each hemoglobin molecule, Hb_4, is replaced by four independent heme groups, 4Hb. The basic one-step reaction is

$$Hb + O_2 \rightleftarrows HbO_2. \tag{1}$$

The local chemical state is specified by values of the molar densities N_{Hb}, N_O, and N_{HbO}. At a given point, these densities will change with time, due to diffusion and to the chemical reaction. The rates of change due to the reaction, denoted by $(\partial/\partial t)_R$, have the form

$$(\partial N_{Hb}/\partial t)_R = -\Gamma,\ (\partial N_O/\partial t)_R = -\Gamma,\ (\partial N_{HbO}/\partial t)_R = \Gamma. \tag{2}$$

Here $\Gamma = \Gamma(N_{Hb}, N_O, N_{HbO})$ is the reaction rate. In the determination of Γ, the strongest experimental constraint comes from equilibrium data. That is, $\Gamma = 0$ must yield the measured dissociation curve for hemoglobin. This curve is fit well by the Hill equation, so we require $\Gamma = 0$ to give

$$S = \frac{(P/P_{50})^n}{1 + (P/P_{50})^n}. \tag{3}$$

Here

$$S = N_{HbO}/(N_{Hb} + N_{HbO}) \tag{4}$$

is the fractional saturation, P is the partial pressure of oxygen, P_{50} is the value of P for equilibrium at 50% saturation, and n is a dimensionless exponent. For our purposes, it is more convenient to write the Hill equation in terms of molar densities. If B_U is the Bunson solubility coefficient in the red cell, then $N_O = B_U P$ and the density at 50% saturation is $N_{50} = B_U P_{50}$. Then Eq. 3 can be written as

$$S = \frac{(N_O/N_{50})^n}{1 + (N_O/N_{50})^n}. \tag{5}$$

There is an infinity of functions Γ for which $\Gamma = 0$ yields Eq. 5. In the absence of extensive experimental kinetics data, a certain arbitrariness in the choice of Γ is inevitable. To proceed, we assume that Γ may be written as a recombination rate Γ_R minus a dissociation rate Γ_D, with functional arguments as follows:

$$\Gamma(N_{Hb}, N_O, N_{HbO}) = \Gamma_R(N_{Hb}, N_O) - \Gamma_D(N_{HbO}). \tag{6}$$

For the dissociation reaction, we assume a rate proportional to concentration

$$\Gamma_D = kN_{HbO}. \tag{7}$$

Then the requirement that $\Gamma = 0$ yield the Hill Eq. 5 gives (uniquely)

$$\Gamma_R = kN_{Hb}(N_O/N_{50})^n. \tag{8}$$

The final expression for Γ may be written as

$$\Gamma = kN_T[(1 - S)C^n - S], \tag{9}$$

where

$$N_T = N_{Hb} + N_{HbO} \tag{10}$$

is the total heme density, and

$$C = N_O/N_{50} \tag{11}$$

is a normalized oxygen concentration.

The idea of constraining Γ by the dissociation curve is due to Moll (1969), and was also used later by Sheth and Hellums (1980) and by Baxley and Hellums (1983). The expressions used for Γ by these authors have the property that $\Gamma \to \infty$ as $C \to 0$, and, for that reason, the expression (Eq. 9) is perhaps to be preferred. Of course the question of the correct Γ, among the infinitely many consistent with the dissociation curve, is an experimental one. Fortunately, the calculated results for the distribution of oxygen in an unloading red cell do not seem to be very sensitive to the choice of Γ, as long as compatibility with the dissociation curve is maintained.

Transport Equations

The transport equations for the three species are obtained by mass balances. In general, the processes entering the mass balance are convection, diffusion, and the chemical reaction. In the present work, we do not consider the convective effects of internal flow within the red cell. We limit attention to cells undergoing, at most, translation and rigid rotation, and we write the equations in the rest frame

of the cell. Then we have

$$\partial N_O/\partial t = D_O\nabla^2 N_O - \Gamma, \tag{12}$$

$$\partial N_{Hb}/\partial t = D_{Hb}\nabla^2 N_{Hb} - \Gamma, \tag{13}$$

and

$$\partial N_{HbO}/\partial t = D_{HbO}\nabla^2 N_{HbO} + \Gamma, \tag{14}$$

where we have assumed that the diffusivities D_O, D_{Hb}, and D_{HbO} are constant.

Because the heme group is so much larger than the oxygen molecule, we may take $D_{HbO} = D_{Hb}$ with a high degree of accuracy. This in turn leads to a major simplification. By adding Eqs. 13 and 14, we get an equation for the total heme density $N_T = N_{Hb} + N_{HbO}$

$$\partial N_T/\partial t = D_{Hb}\nabla^2 N_T. \tag{15}$$

Since the red-cell membrane does not pass hemoglobin, there can be no flux of N_T across the boundary. Thus an initially uniform distribution of total hemoglobin will remain uniform for all times. From here on, we assume that N_T is constant. Then Eqs. 12–14 reduce to two independent equations, which are conveniently written in terms of the saturation S (Eq. 5) and the normalized oxygen density C (Eq. 11)

$$\partial S/\partial t = D_{Hb}\nabla^2 S + k[(1 - S)C^n - S], \tag{16}$$

and

$$\partial C/\partial t = D_O\nabla^2 C - k[N_T/N_{50}][(1 - S)C^n - S]. \tag{17}$$

To complete the formulation of any particular problem, we need initial conditions and boundary conditions. Consider first the initial conditions. It is possible to deal with an arbitrary initial state, but that is a needless complexity. A red cell may lose some of its oxygen in its precapillary travels, but it is very unlikely that such loss will be both severe and rapid enough to create a spatially inhomogeneous state in the red cell before it gets to the capillary. Thus we may assume that the red cell enters the capillary with uniform values of S and C, say S_0 and C_0, related by the equilibrium condition $S_0 = C_0^n/(1 + C_0^n)$.

Now consider the boundary conditions. Since no hemoglobin can pass through the cell membrane, we have $\mathbf{n} \cdot \nabla S = 0$ on the boundary, $\mathbf{n}$ being the unit normal to the boundary. The remaining boundary condition depends on the situation being modeled. Consider some examples. To mimic the environment seen by a red cell as it moves down a capillary, we could impose on the boundary a value of C that decreases with time. Alternatively, we could model the same situation by imposing a value of oxygen flux (proportional to $\mathbf{n} \cdot \nabla C$) on the boundary. A more complicated situation can arise if the red cell and its environment are being analyzed simultaneously. Then one must solve transport equations outside the red cell, as well as solving Eqs. 16 and 17 in the red cell. We still have $\mathbf{n} \cdot \nabla S = 0$ on the boundary, but the condition on C is replaced by two matching conditions. One matching condition is continuity of the oxygen flux $\mathbf{n} \cdot D_O\nabla N_O$. The second matching condition depends on whether there is any resistance to oxygen flow across the red-cell membrane. Huxley and Kutchai (1983) have recently reexamined this question and have concluded that the membrane resistance is small. In the absence of such resistance, the oxygen partial pressure, N_O/B_U, will be continuous across the boundary.

Parameter Values

A range of parameter values has been used in previous theoretical studies. While a critical review of such values, leading to a "canonical" red cell, would be most useful, it is beyond the scope of the present work. For the most part, we select values that are typical of recent work. None of our general conclusions are sensitive to the exact values of the parameters.

Consider first the kinetic parameters. We start with the total heme concentration, which may be calculated from the hemoglobin density within the red cell. For this number we use 340 g/l (Wintrobe et al. 1981). For a hemoglobin molecular weight of 67,000 this gives a heme concentration of

$$N_T = 2.03 \times 10^{-5}\ \text{mol/cm}^3, \tag{18}$$

close to the values used by Moll (1969) and Kutchai (1970), 2.0×10^{-5}, and by Sheth and Hellums (1980) and Baxley and Hellums (1983), 2.2×10^{-5}. The constants n and P_{50} in the Hill equation (Eq. 3) were obtained by direct nonlinear regression applied to the table of values given by Honig (1981), for a temperature of 37°C and a pH of 7.4. The values are

$$P_{50} = 26.4\ \text{mmHg}, n = 2.65. \tag{19}$$

The conversion of P_{50} to N_{50} requires a value for the Bunson solubility coefficient B_U. A useful discussion of this quantity has been given by Spaan et al. (1980). They give a formula (their Eq. 10) that relates B_U to B_{UW}, the Bunson coefficient for water, with corrections for hemoglobin concentration and salt concentration. The corrections for salt concentration are generally small (a few percent) so we ignore them. Then the formula of Spaan et al. (1980) reduces to

$$B_U = B_{UW}(1 + 0.000312[\text{Hb}]), \tag{20}$$

where [Hb] is the hemoglobin density in grams per liter, 340 in our case. B_{UW} may be computed from standard tables (Linke, 1965) to be 1.41×10^{-9} mol/mmHg/cm^3 at 37°C. Then $B_U = 1.56 \times 10^{-9}$ mol/mmHg/cm^3 and

$$N_{50} = P_{50}B_U = 4.12 \times 10^{-8}\ \text{mol/cm}^3. \tag{21}$$

The last kinetic parameter we need is the dissociation rate constant, k. We follow other authors and use here the value

$$k = 44\ \mathrm{s}^{-1}, \tag{22}$$

based on the work of Gibson et al. (1955).

We take the diffusion coefficients D_O and D_{Hb} from the recent measurements of Spaan et al. (1980). They give $D_{Hb} = 1.0 \times 10^{-7}\ \mathrm{cm}^2/\mathrm{s}$ at 25°C for [Hb] = 340 g/l. The correction to 37°C may be made on the basis of the work of Keller et al. (1971), whose measurements show that, at high hemoglobin concentrations (315 g/l), D_{Hb} increases by a factor of 1.44 as T goes from 25 to 37°C. Using this temperature correction factor, we get

$$D_{Hb} = 1.44 \times 10^{-7}\ \mathrm{cm}^2/\mathrm{s}. \tag{23}$$

For the oxygen diffusion coefficient, Spaan et al. (1980) give $D_O = 7.3 \times 10^{-6}\ \mathrm{cm}^2/\mathrm{s}$ at 25°C for [Hb] = 340 g/l. As discussed by Wittenberg (1970), the temperature dependence of D_O is about the same in water as in tissue. Then we may use the data summarized by Himmelblau (1964, Fig. 9) that show that D_O in water increases by a factor of ~1.3 as T increases from 25 to 37°C. Using this factor with the value above, we get

$$D_O = 9.5 \times 10^{-6}\ \mathrm{cm}^2/\mathrm{s}. \tag{24}$$

In the scale analysis to be carried out below, we need a typical red-cell dimension a. More precisely, a should be a typical diffusion path length from cell midplane to cell boundary. To estimate an average value of a, we imagine the red cell to be a cylindrical disk of thickness $2a$, radius r, and volume V. Then $a = V/(2\pi r^2)$, and we use the average values measured by Evans and Fung (1972), namely $r = 3.91\ \mu\mathrm{m}$ and $V = 94\ \mu\mathrm{m}^3$, to get $a \approx 1\ \mu\mathrm{m}$. We use this value in the scale analyses below.

Time Scales

We begin by rewriting the transport equations (Eqs. 16 and 17). We use the characteristic red-cell dimension a to make the Laplacian operators dimensionless. Then Eqs. 16 and 17 can be written as

$$\partial S/\partial t = \nabla^2 S/\tau_{DS} + \gamma/\tau_{KS} \tag{25}$$

and

$$\partial C/\partial t = \nabla^2 C/\tau_{DC} - \gamma/\tau_{KC}, \tag{26}$$

where

$$\gamma = (1 - S)C^n - S. \tag{27}$$

The four time scales appearing in Eqs. 26 and 27 are the kinetic time scales $\tau_{KS} = k^{-1}$ and $\tau_{KC} = (kN_T/N_{50})^{-1}$, and the diffusion time scales $\tau_{DS} = a^2/D_{Hb}$ and $\tau_{DC} = a^2/D_O$.

The character of the solution depends on the relative sizes of these four time scales. The most important single question about the nature of the solution is whether or not the S and C distributions are in (or near) local chemical equilibrium. A simple scale analysis of Eqs. 25 and 26 (first carried out in this context by Keller and Friedlander, 1966) shows that deviations from chemical equilibrium will occur on a spatial scale δ, given by

$$(\delta/a)^2 \sim [(\tau_{DS}/\tau_{KS}) + (\tau_{DC}/\tau_{KC})]^{-1}. \tag{28}$$

If $\delta \geq a$, then deviations from chemical equilibrium can occur throughout the red cell. If, on the other hand, $\delta \ll a$, then the bulk of the interior of the red cell will be in equilibrium, and, near the cell wall, there will be a boundary layer of thickness, δ, where deviations from chemical equilibrium occur. From Eq. 28 we see that a necessary and sufficient condition for $\delta \ll a$ is that at least one of the kinetic times be much shorter than the corresponding diffusion time. We may easily check this for the red-cell parameters given previously. For $a = 1\ \mu\mathrm{m}$, we get $\tau_{DS} = 69.4$ ms, $\tau_{KS} = 22.7$ ms, $\tau_{DC} = 1.05$ ms, and $\tau_{KC} = 46.1\ \mu$s. Hence $\tau_{DS}/\tau_{KS} = 3.06$ and $\tau_{DC}/\tau_{KC} = 22.8$, and we do have a boundary layer situation.

One of the main goals of the theory developed here is to determine the relation between time scales of physiological importance and the above four intrinsic time scales of the red cell. One such time scale is the internal oxygen transport time τ_I, that is, the time required for a change in oxygen distribution within the red cell. We may get a simple estimate of τ_I by observing that, in a boundary layer situation such as we have, the bulk of the red cell will be near equilibrium with respect to the C and S distributions. By adding τ_{KS} times Eq. 25 to τ_{KC} times Eq. 26, and by using the equilibrium relation $S = F(C) = C^n/(1 + C^n)$, we get the following approximate equation for the interior oxygen distribution

$$[\tau_{KC} + \tau_{KS}F'(C)](\partial C/\partial t) \approx \nabla \cdot \{[\tau_{KC}/\tau_{DC} + (\tau_{KS}/\tau_{DS})F'(C)]\nabla C\}. \tag{29}$$

Although $F'(C)$ is variable, it is of order one in most of the saturation range of interest. Then we infer from Eq. 29 that the internal time scale for transporting oxygen within the red cell is

$$\tau_I = \frac{\tau_{KC} + \tau_{KS}}{\tau_{KS}/\tau_{DS} + \tau_{KC}/\tau_{DC}}. \tag{30}$$

For the numerical parameters used above, we have $\tau_I = 0.0613$ s for $a = 1\ \mu$m. For some purposes, it is convenient to express the transport time in terms of an effective diffusivity D_E, defined by $\tau_I = a^2/D_E$. Then

$$D_E = (\tau_{KC}D_O + \tau_{KS}D_{Hb})/(\tau_{KC} + \tau_{KS}). \tag{31}$$

Thus the effective diffusivity is a weighted average of the oxygen and hemoglobin diffusivities, with the weights being the kinetic time scales.

The most important physiological time scale is the unloading time τ_U, that is, the time required to unload a significant fraction of the oxygen from the red cell. Note that the unloading time, τ_U, can be longer than the transport time, τ_I, discussed above. It depends on the transport resistance of the boundary layer at the red-cell membrane. If the boundary layer resistance is small, then $\tau_U \sim \tau_I$. If, on the other hand, there is significant resistance in the boundary layer, then $\tau_U > \tau_I$. As we shall see in the next section, the boundary layer resistance is significant, and the unloading time for the red cell is, in fact, somewhat longer than the transport time.

ASYMPTOTIC THEORY

Nature of the Boundary Layer Solution

Before beginning the actual analysis, it is helpful to consider the qualitative nature of the solution. In the interior of the red cell, there is chemical equilibrium to a first approximation, and the S and C distributions satisfy Eq. 29 and the equilibrium relation (Eq. 5). This interior equilibrium solution must break down near the boundary. This can be seen easily by noting that, on the boundary, $\mathbf{n} \cdot \nabla S = 0$ (hemoglobin does not leave the cell) but $\mathbf{n} \cdot \nabla C \neq 0$ (there is an oxygen flux). Thus S and C cannot satisfy the functional relation of equilibrium on or near the boundary. The boundary layer in which this deviation from equilibrium occurs is the region in which the total oxygen flux, facilitated plus free, is converted to the free flux, which leaves the cell. The nature of the boundary layer depends on the four time scales that appear in Eqs. 25 and 26—more precisely, on three dimensionless ratios of these time scales, which we take to be

$$R_C = \tau_{DC}/\tau_{KC},\ R_S = \tau_{DS}/\tau_{KS},\ \lambda = \tau_{KS}/\tau_{KC}. \tag{32}$$

As discussed in the Time Scales section, the basic condition for the existence of a boundary layer is that at least one of R_C, R_S be large. A detailed scale analysis shows that there are six qualitatively different solutions corresponding to six different regions in the R_C, R_S, λ space. Most of the six regions are not physiologically relevant, however. If we use the parameter values given previously and consider a range of cell sizes, we find only two qualitatively different solutions, corresponding to either $R_S \gg \sqrt{R_C}$ or $R_S \ll \sqrt{R_C}$, with $R_C \gg R_S$ and $\lambda > 1$ in both cases. We summarize now the properties of the solutions in these cases.

For $R_S \gg \sqrt{R_C}$, the drop in oxygen across the boundary layer, $(\Delta C)_{BL}$, is small: $(\Delta C)_{BL} \sim \sqrt{R_C}/R_S$. The change in the normal gradient, however, is $(\Delta \partial S/\partial n)_{BL} = O(1)$. Thus, in this parameter range, the purpose of the boundary layer is to correct the interior value of $\partial S/\partial n$. The interior value of C, on the other hand, needs no correction in the first approximation. Because the boundary layer resistance is small in this case, we expect that the unloading and adjustment times will be comparable. This is borne out by detailed estimates, which show that $\tau_I \sim \tau_U \sim \tau_{DS}$, that is, the characteristic time is of the order of the hemoglobin diffusion time.

Consider now the second case, $R_S \ll \sqrt{R_C}$. In this case $(\Delta C)_{BL} = O(1)$ and $(\Delta \partial S/\partial n)_{BL} \sim R_S/\sqrt{R_C} \ll 1$. Thus there is an appreciable change in C across the boundary layer. This means that the resistance to diffusion in the boundary layer is significant, and we expect that the unloading time may exceed the adjustment time. Detailed estimates confirm this: $\tau_I \sim \tau_{DS}$ and $\tau_U \sim (\sqrt{R_C}/R_S)\tau_{DS} > \tau_I$. There are two consequences of the inequality $\tau_U > \tau_I$. First, the interior profile will be rather flat, because the leak of oxygen out is slower than the rearrangement of oxygen within. Second, there is a possibility of a lumped-parameter description of the unloading, which would mean that the set of partial differential equations could in effect be replaced by a single first-order ordinary differential equation.

For large cells, the first case above ($R_S \gg \sqrt{R_C}$) is relevant. For small cells we have the second case ($R_S \ll \sqrt{R_C}$). For the parameter values given previously, the boundary between these regions, namely $R_S = \sqrt{R_C}$, corresponds to a cell size $a \approx 1.6$ μm. For our adopted standard value of $a = 1$ μm, the relevant case is then the second one, $R_S \ll \sqrt{R_C}$. However, the large parameters in the theory are not compellingly large for the red cell. For $a = 1$ μm we have $R_S = 3.06$ and $R_C = 22.8$, so that some faith is required to base a calculation on $R_S \ll \sqrt{R_C}$. As it turns out the theory gives better results than one might expect. To establish this, we have taken a one-dimensional slab model as a test case. We developed the detailed boundary layer theory for three parameter orderings: $R_S \ll \sqrt{R_C}$, $R_S \sim \sqrt{R_C}$, and $R_S \gg \sqrt{R_C}$. We then solved the exact equations by a finite difference method. A comparison of the numerical results showed that for $a = 1$ μm, the boundary layer theory based on $R_S \ll \sqrt{R_C}$ agrees best with the exact solution, so only that case is considered further here.

To carry out the boundary layer analysis, it is necessary to choose a large parameter and then order the terms in the equations with respect to this parameter. We take the basic large parameter to be R, where

$$R_C = R^2. \tag{33}$$

Now we order the other parameters. We begin with R_S. Since we are dealing with the case $R_S \ll R$, we take the simplest ordering, namely,

$$R_S = O(1). \tag{34}$$

There are other possibilities, such as $R_S = O(R^{1/2})$. We have developed the theory with this ordering, but it offers no advantages over the simpler ordering (Eq. 34). The unloading time is

$$\tau_U \sim (\sqrt{R_C}/R_S)\tau_{DS} = R\tau_{KS}. \tag{35}$$

To account for this, we introduce a new dimensionless time variable τ, given by

$$\tau = t/(R\tau_{KS}). \tag{36}$$

Finally we must order λ. We have $\lambda = 492$, which, for $a = 1$ μm, is close to R^4. Thus we can take λ to be proportional to R^4

$$\lambda = \alpha R^4. \tag{37}$$

Then Eqs. 25 and 26 become

$$\partial S/\partial\tau = (R/R_S)\nabla^2 S + R\gamma \tag{38}$$

and

$$\partial C/\partial\tau = \alpha R^3(\nabla^2 C - R^2\gamma). \tag{39}$$

We will study the asymptotic solution of these equations in the limit $R \to \infty$ at fixed α and R_S. This is carried out below and the results then are compared with the finite difference solutions.

Solution of the Boundary Layer Equations

The solutions S and C depend on position r, time τ, and the parameters R, α, and R_S. In the interior, we seek expansions useful for large R at fixed r, τ, α, and R_S. We use a subscript I to denote this interior solution. We seek solutions in inverse powers of R

$$S = S_I^{(0)} + R^{-1}S_I^{(1)} + R^{-2}S_I^{(2)} + \dots \tag{40}$$

and

$$C = C_I^{(0)} + R^{-1}C_I^{(1)} + R^{-2}C_I^{(2)} + \dots . \tag{41}$$

Substitution of these expansions into Eqs. 38 and 39 leads to a sequence of equations for $S_I^{(j)}$ and $C_I^{(j)}$. In writing the γ terms in the equations, it is convenient to use the following notation

$$\gamma_I = \gamma_I^{(0)} + R^{-1}\gamma_I^{(1)} + R^{-2}\gamma_I^{(2)} + \dots , \tag{42}$$

where

$$\gamma_I^{(0)} = (1 - S_I^{(0)})(C_I^{(0)})^n - S_I^{(0)}, \tag{43}$$

and

$$\gamma_I^{(1)} = -\{1 + [C_I^{(0)}]^n\}S_I^{(1)} + n[C_I^{(0)}]^{n-1}[1 - S_I^{(0)}]C_I^{(1)}, \tag{44}$$

with a similar but lengthier expression for $\gamma_I^{(2)}$. With this notation, the first three S-equations are

$$\nabla^2 S_I^{(0)} + R_S\gamma_I^{(0)} = 0, \tag{45}$$

$$\nabla^2 S_I^{(1)} + R_S\gamma_I^{(1)} = R_S[\partial S_I^{(0)}/\partial\tau], \tag{46}$$

and

$$\nabla^2 S_I^{(2)} + R_S\gamma_I^{(2)} = R_S[\partial S_I^{(1)}/\partial\tau]. \tag{47}$$

The first three C-equations are

$$\gamma_I^{(0)} = 0, \tag{48}$$

$$\gamma_I^{(1)} = 0, \tag{49}$$

and

$$\nabla^2 C_I^{(0)} = \gamma_I^{(2)}. \tag{50}$$

Then the zero-order interior problem may be put into the form

$$\nabla^2 S_I^{(0)} = 0 \tag{51}$$

and

$$C_I^{(0)} = \{S_I^{(0)}/[1 - S_I^{(0)}]\}^{1/n}. \tag{52}$$

The first-order interior problem can be written as

$$\nabla^2 S_I^{(1)} = R_S[\partial S_I^{(0)}/\partial\tau] \tag{53}$$

and

$$C_I^{(1)} = \frac{1 + [C_I^{(0)}]^n}{n[C_I^{(0)}]^{n-1}[1 - S_I^{(0)}]} S_I^{(1)}. \tag{54}$$

The Laplace equation (Eq. 51) and the Poisson equation (Eq. 53) are straightforward to solve. However, the boundary conditions are not known at this point. We must use the true boundary conditions and the analysis of the boundary layer to get the effective boundary conditions for the interior problems (Eqs. 51–54).

Consider now the boundary layer near the red-cell membrane. From Eqs. 28 and 32–34 we find that the boundary layer thickness is $\delta/a = O(R^{-1})$. To resolve this boundary layer, we introduce new coordinates appropriate both to the geometry of the boundary and to the scale δ. We let ξ_1, ξ_2 be orthogonal coordinates in the surface of the red-cell membrane, and we let $\mathbf{r}_W(\xi_1, \xi_2)$ be the position vector to a point ξ_1, ξ_2 in the wall. We then extend the surface coordinates ξ_1, ξ_2 into a three-dimensional coordinate system by introducing a scaled normal coordinate η, such that the position vector $\mathbf{r}$ is given by

$$\mathbf{r} = \mathbf{r}_W(\xi_1, \xi_2) + (\eta/R)\mathbf{n}(\xi_1, \xi_2). \tag{55}$$

Here $\mathbf{n}$ is a unit normal at ξ_1, ξ_2 pointing from the wall toward the cell interior, and η has been scaled so that the thickness of the boundary layer corresponds to $\Delta\eta = O(1)$.

To write the equations in terms of the new coordinates, we must transform the Laplacian operator. We forego the details of that lengthy exercise in differential geometry and just give the result

$$\nabla^2 = R^2(\partial^2/\partial\eta^2) - R(\kappa_1 + \kappa_2)(\partial/\partial\eta) - \eta(\kappa_1^2 + \kappa_2^2)(\partial/\partial\eta) + \nabla_W^2 + O(R^{-1}). \tag{56}$$

Here $\kappa_1(\xi_1, \xi_2)$ and $\kappa_2(\xi_1, \xi_2)$ are the principal curvatures of the boundary surface at ξ_1, ξ_2. The surface Laplacian

∇_W^2 is given by

$$\nabla_W^2 = \frac{1}{h_1 h_2}\frac{\partial}{\partial \xi_1}\left(\frac{h_2 \partial}{h_1 \partial \xi_1}\cdot\right) + \frac{\partial}{\partial \xi_2}\left(\frac{h_1 \partial}{h_2 \partial \xi_2}\cdot\right), \tag{57}$$

where h_1 and h_2 are the scale factors for the orthogonal surface coordinates ξ_1, ξ_2.

To study the solution near the boundary, in the limit $R \to \infty$, we again take expansions in inverse powers of R. This time, however, the expansions are at fixed ξ_1, ξ_2, and η, rather than at fixed $\mathbf{r}$. We use a subscript B to denote these boundary layer functions. Then the expansions are

$$S = S_B^{(0)} + R^{-1}S_B^{(1)} + R^{-2}S_B^{(2)} + \ldots \tag{58}$$

and

$$C = C_B^{(0)} + R^{-1}C_B^{(1)} + R^{-2}C_B^{(2)} + \ldots. \tag{59}$$

Here $S_B^{(j)}$ and $C_B^{(j)}$ are functions of ξ_1, ξ_2, η, and τ (and the parameters α and R_S). The expression, Eq. 56, and the expansions, Eqs. 58 and 59, are substituted into the basic Eqs. 38 and 39. The result is a sequence of equations for $S_B^{(j)}$ and $C_B^{(j)}$. We begin the analysis with the first two S-equations

$$\partial^2 S_B^{(0)}/\partial \eta^2 = 0, \tag{60}$$

and

$$\partial^2 S_B^{(1)}/\partial \eta^2 = (\kappa_1 + \kappa_2)\partial S_B^{(0)}/\partial \eta. \tag{61}$$

The boundary condition $\mathbf{n} \cdot \nabla S = 0$ on the wall translates to

$$\partial S_B^{(j)}/\partial \eta = 0 \text{ at } \eta = 0 \text{ for all j}. \tag{62}$$

It follows that

$$S_B^{(0)} = A_B^{(0)}, S_B^{(1)} = A_B^{(1)} \tag{63}$$

where the As may depend on ξ_1, ξ_2, and τ, but not η. The connection between the S_B and S_I solutions is obtained by asymptotic matching (as described, for example, in Van Dyke, 1975). By matching the two-term boundary expansion $S_B^{(0)} + R^{-1}S_B^{(1)}$ with the one-term interior expansion, we get

$$S_I^{(0)}|_W = A_B^{(0)}$$

and

$$\mathbf{n} \cdot \nabla S_I^{(0)}|_W = 0, \tag{64}$$

where subscript W means evaluated at the wall.

Because $S_I^{(0)}$ is harmonic (Eq. 51) and has zero normal derivative on the boundary, it is necessarily a constant in space. Thus

$$S_I^{(0)} = S_B^{(0)} = A_B^{(0)} = A(\tau). \tag{65}$$

That is, to lowest order, there are no saturation gradients within the red cell. It is only in order R^{-1} that saturation gradients appear.

To proceed further, we consider the equation for $C_B^{(0)}$

$$\partial^2 C_B^{(0)}/\partial \eta^2 = \gamma_B^{(0)} = \{[1 - S_B^{(0)}][C_B^{(0)}]^n - S_B^{(0)}\}. \tag{66}$$

By multiplying Eq. 66 with $\partial C_B^{(0)}/\partial \eta$, we may integrate the equation once. The constant of integration is evaluated by using the fact that $(\partial C_B^{(0)}/\partial \eta) \to 0$ as $\eta \to \infty$, and by matching $C_B^{(0)}$ and $C_I^{(0)}$. The result is

$$\frac{1}{2}\left[\frac{\partial C_B^{(0)}}{\partial \eta}\right]^2 = \frac{1 - A}{n+1}\{[C_B^{(0)}]^{n+1} - [C_I^{(0)}|_W]^{n+1}\} - A[C_B^{(0)} - C_I^{(0)}|_W]. \tag{67}$$

By evaluating Eq. 67 at $\eta = 0$, we get a relation between the dimensionless flux

$$q = \partial C_B^{(0)}/\partial \eta \quad \text{at} \quad \eta = 0, \tag{68}$$

the specified value of C at the wall, C_W, and the value of the interior solution at the wall, $C_I^{(0)}|_W$. By using the equilibrium relation between $C_I^{(0)}$ and $S_I^{(0)}$ (Eq. 52), we may express q entirely in terms of $A = S_I^{(0)}$ and C_W

$$q = \left[\frac{2(1 - A)}{n+1}C_W^{n+1} - 2AC_W + \frac{2An}{n+1}\left(\frac{A}{1 - A}\right)^{1/n}\right]^{1/2}. \tag{69}$$

Eq. 69, which gives the flux in terms of the cell saturation A, and the boundary value of oxygen C_W, is the basis for the lumped parameter description of the unloading process.

The cell saturation $A(\tau)$ is still undetermined. It turns out that we must deal with $S_B^{(2)}$ in order to find $A(\tau)$. The equation for $S_B^{(2)}$ may be reduced to

$$\partial^2 S_B^{(2)}/\partial \eta^2 + R_S \gamma_B^{(0)} = 0. \tag{70}$$

We may use Eq. 66 to eliminate $\gamma_B^{(0)}$. Integration of the resulting equation gives

$$S_B^{(2)} = -R_S C_B^{(0)} + A_B^{(2)} + B_B^{(2)}\eta, \tag{71}$$

where $A_B^{(2)}$ and $B_B^{(2)}$ are independent of η. By applying the boundary condition $\partial S_B^{(2)}/\partial \eta = 0$ at $\eta = 0$, we get

$$B_B^{(2)} = R_S q. \tag{72}$$

Finally, we match the three-term inner expansion $S_B^{(0)} + R^{-1}S_B^{(1)} + R^{-2}S_B^{(2)}$ with the two-term outer expansion $S_I^{(0)} + R^{-1}S_I^{(1)}$. This yields Eq. 64 again, plus the new result

$$\mathbf{n} \cdot \nabla S_I^{(1)}|_W = B_B^{(2)} = R_S q. \tag{73}$$

Now we use the interior Eqs. 46 and 49. By integrating Eq. 46 over the volume occupied by the red cell and by using the divergence theorem, we get

$$V(\mathrm{d}A/\mathrm{d}\tau) = -(1/R_S)\iint_W \mathbf{n}\cdot\nabla S_1^{(1)}\mathrm{d}\sigma = -\iint_W q\mathrm{d}\sigma, \quad (74)$$

where V is the cell volume and $\mathbf{n}$ is the interior normal. Let A_W be the surface area of W, and let $L = V/A_W$. Then Eq. 74 can be written as

$$\mathrm{d}A/\mathrm{d}\tau = -\langle q\rangle/L, \quad (75)$$

where

$$\langle q\rangle = (1/A_W)\iint_W q\mathrm{d}\sigma \quad (76)$$

is the surface-averaged flux.

Eqs. 75 and 76 give a lumped-parameter description of the red-cell unloading. Calculations based on this description proceed as follows. Given the cell saturation A at a particular time τ, and the distribution of boundary values $C_W(\xi_1, \xi_2, \tau)$, we calculate $\langle q\rangle$, using Eq. 69 for q. Then the saturation may be stepped forward in time by Eq. 75, and the process repeated. In the special case when C_W depends on time but not position, $\langle q\rangle = q$, and Eq. 75 reduces to a first-order ordinary differential equation for $A(\tau)$.

Comparison of Numerical and Boundary Layer Solutions

To test the accuracy of the boundary layer theory, we have compared its predictions with numerical solutions of the full equations. This has been done for slab models of red cells, in which the solution depends only on a single spatial coordinate x. The characteristic scale a in this case is the half-thickness of the slab, and the dimensionless coordinate x is in the range $-1 \le x \le 1$.

Numerical solutions of Eqs. 38 and 39 have been described in detail by a number of authors (Moll, 1969; Kutchai, 1970; Sheth, 1979; Sheth and Hellums, 1980; Baxley and Hellums, 1983; and Federspiel, 1983). For that reason, the description of our procedure here is brief. We used a finite difference method, with the diffusion terms treated implicitly, and the nonlinear kinetic terms treated explicitly. A spatially uniform grid was used, with the number of grid points being between 20 and 200 in half the slab. In most runs, 50 points were used. The time step was limited by stability rather than accuracy, and was typically 10^{-4} times the unloading time τ_U.

To compare the two theories, we have used each to compute the mean saturation

$$\langle S\rangle = \left(\frac{1}{2}\right)\int_{-1}^{1} S\mathrm{d}x \quad (77)$$

and the flux

$$F = \partial C/\partial x \quad \text{at} \quad x = 1, \quad (78)$$

as functions of the scaled time τ. This has been done for a cell half-width $a = 1$ μm, an initial saturation of 0.9, and two boundary oxygen concentrations: $C_W = 0.8$, corresponding to an oxygen tension of ~21 mmHg, and $C_W = 0.0$, corresponding to the maximum possible oxygen demand. Fig. 1 shows $\langle S\rangle$ as a function of the dimensionless time τ for $C_W = 0.8$ (curves 1), and for $C_W = 0.0$ (curves 2). In each case, the solid curve is from the numerical solution and the dashed curve is from the boundary layer solution. The agreement is very good. The maximum absolute error in $\langle S\rangle$ is 0.010 for $C_W = 0.8$, and 0.024 for $C_W = 0.0$. Fig. 2 shows the dimensionless flux F as a function of time τ. Again the agreement is very good. The maximum absolute error in F is 0.043 for $C_W = 0.8$ (curves 1), and 0.100 for $C_W = 0.0$ (curves 2).

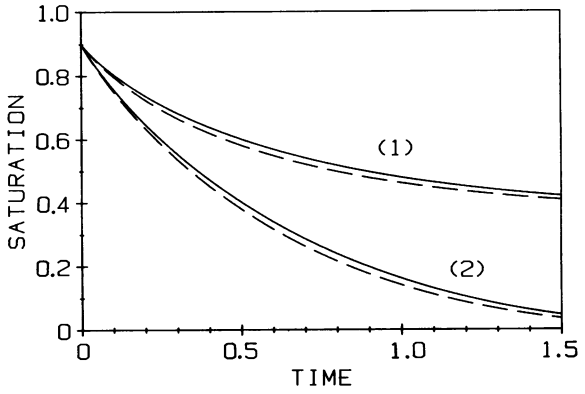

FIGURE 1 Mean saturation $\langle S\rangle$ as a function of dimensionless time τ for a cell half-width of 1 μm, and initial saturation of 0.9. The solid curves are from the numerical solution of the full equations and the dashed curves are from the boundary layer theory. Case *1* is for a boundary oxygen concentration $C_W = 0.8$ (corresponding to an oxygen tension of ~21 mmHg), and case *2* is for $C_W = 0.0$. Scaling: $\tau = 1$ corresponds to a time of 0.108 s.

It is also of interest to see how the accuracy of the boundary layer theory depends on the cell size a. To check this, we have calculated the unloading time, somewhat

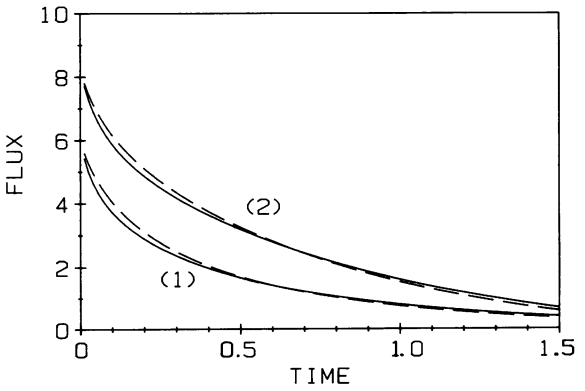

FIGURE 2 Dimensionless oxygen flux F as a function of dimensionless time τ for a cell half-width of 1 μm, and initial saturation of 0.9. The solid curves are from the numerical solution of the full equations, and the dashed curves are from the boundary layer theory. Case *1* is for a boundary oxygen concentration $C_W = 0.8$, and case *2* is for $C_W = 0.0$. Scaling: $\tau = 1$ corresponds to a time of 0.108 s, and $F = 1$ to a flux of 3.91×10^{-9} mol/cm^2 s.

arbitrarily defined as the time required for the mean saturation to drop from 0.9 to 0.3 when $C_W = 0.0$ on the boundary. With the scaling (Eq. 36) for time, which depends on a, the dimensionless unloading time predicted by the boundary layer theory is the same for all a. In fact we get from Eqs. 69 and 75 the following simple result for the unloading time

$$\int_{0.3}^{0.9} \{[2n/(n+1)][A/(1-A)]^{1/n}A\}^{-1/2}dA = 0.6295. \quad (79)$$

This is the dashed line in Fig. 3. The solid curve gives the exact unloading time from the numerical solution. The two results differ by <10% in the range $0.4 \le a \le 1.2$ μm, and the boundary layer theory is probably best in that range of cell sizes. The errors in Fig. 3 appear larger than those in Figs. 1 and 2. This is just a consequence of the flatness of the $\langle S \rangle$ v. τ curves. For $a = 1$ μm, for example, the error in the unloading time is 7.6%, whereas the maximum error in saturation (for $C_W = 0.0$) is only 0.024.

The boundary layer theory is somewhat less successful in its prediction of detailed spatial profiles. In lowest order, the theory predicts a uniform saturation profile, whereas the numerical solution shows spatial variations. Consider, for example, the case of $a = 1$ μm, with initial saturation of 0.9, and boundary oxygen $C_W = 0.8$. When the mean saturation of the numerical solution is 0.5 (which happens at $\tau = 0.88$), the actual saturation values vary from 0.52 at the center of the cell to 0.48 at the edge. With the more extreme boundary condition of $C_W = 0.0$, a mean saturation of 0.5 occurs at $\tau = 0.37$, at which time the saturation varies from 0.55 at cell center to 0.43 at cell edge. It is possible to get more accurate profiles from the boundary layer theory by computing higher order terms. However, the main virtue of the boundary layer theory, namely its simplicity, is largely lost when one goes beyond the lowest order.

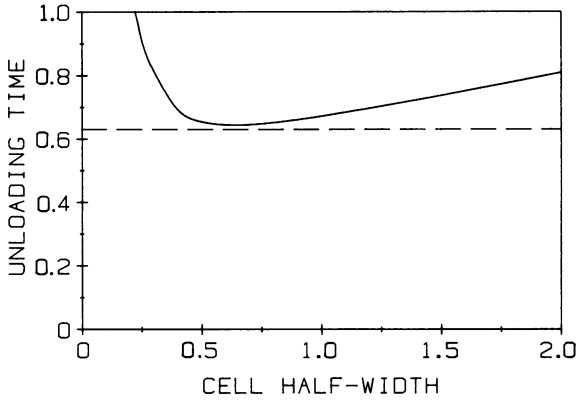

FIGURE 3 Dimensionless unloading time τ as a function of cell half-width in microns. The unloading time is defined as the time required to go from an initial saturation of 0.9 to a mean saturation of 0.3, with zero oxygen tension maintained on the boundary. The solid curve is from the numerical solution of the full equations, and the dashed curve is from the boundary layer theory. Scaling: $\tau = 1$ corresponds to a dimensional time of $0.108(a)$ s, where a is the cell half-width in microns.

The conclusion is that the boundary layer theory gives a very good approximation to global quantities such as mean saturation and unloading times, in the range of cell half-widths $0.4 \le a \le 1.2$ μm. Even in the range $1.2 \le a \le 2.0$ μm, the boundary layer results are sufficiently accurate to be useful.

OXYGEN UNLOADING TIMES

In this section, we use the simple results from the asymptotic analysis to discuss the oxygen unloading time for a red cell. The first step is to unravel the various scalings used in the asymptotic theory and to put the equation for unloading in terms of physically significant quantities. This is done below after which we examine a red cell in a zero oxygen environment in order to calculate the minimum oxygen unloading time.

Since all of the results of this section are obtained from the asymptotic analysis, they are valid only for parameter values consistent with the analysis—that is, for values close to those given previously and for mean cell half-widths between 0.4 μm and 1.2 μm.

Equation for Oxygen Unloading

Oxygen unloading is described by Eqs. 75 and 76. We transform these by using a dimensional time variable t and dimensional lengths. The dependent variable is S, the spatial mean of the saturation. The equation for S is

$$dS/dt = -\langle q \rangle / t_U. \quad (80)$$

Here t_U is a constant given by

$$t_U = L[N_T/(D_O k B_U P_{50})]^{1/2}, \quad (81)$$

where L is the ratio of the cell volume to cell surface area. (The parameter t_U is just our earlier unloading time τ_U with the scale $a = L$.) We use the measured values of Evans and Fung (1972) to get $L = 0.696$ μm. The other quantities appearing in Eq. 81 were all defined previously and we get $t_U = 0.0756$ s. The quantity $\langle q \rangle$ is an average over the surface of the red cell of the function q, given by

$$q = \left\{ \frac{2(1-S)}{n+1} C_W^{n+1} - 2SC_W + \frac{2n}{n+1} \frac{S^{(n+1)/n}}{(1-S)^{1/n}} \right\}^{1/2}. \quad (82)$$

Here $n = 2.65$ is the exponent in the Hill equation, and

$$C_W = P_W/P_{50}, \quad (83)$$

where P_W is the oxygen tension on the red cell boundary. If C_W does not vary with position, then $\langle q \rangle = q$, and Eq. 80 is a first-order ordinary differential equation for S.

It is also of interest to determine F_T, the total flux of oxygen out of the red cell. This is done by transforming Eq. 68 into dimensional form. We get

$$F_T = (N_T/t_U) V \langle q \rangle, \quad (84)$$

where V is the cell volume. For the parameter values given earlier, $F_T = 2.52 \times 10^{-14} \langle q \rangle$ mol/s.

Eqs. 80–84 give a complete description of the oxygen unloading process. Eq. 80 shows that the unloading is governed by the combination of physical parameters contained in t_U, and the function $\langle q \rangle$, which accounts for both the boundary value of oxygen tension and the amplitude dependence of the boundary layer resistance.

Minimum Times for Oxygen Unloading

As emphasized by Hellums (1977), the internal resistance of the red cell to oxygen diffusion is not negligible. The unloading time for a given red cell will depend on both this internal resistance and the external environment. The internal resistance alone, however, determines the minimum possible unloading time. This minimum time is an important intrinsic property of the red cell. It may be calculated easily by using Eqs. 80–83. At the boundary, we take the oxygen tension to be zero, corresponding to the case of maximum possible oxygen demand. With $C_W = 0$, Eq. 80 reduces to

$$\frac{dS}{dt} = -\left\{\frac{1}{t_U}\frac{2n}{n+1}\frac{S^{(n+1)/n}}{(1-S)^{1/n}}\right\}^{1/2}, \qquad (85)$$

with a given initial value $S(0) = S_0$. In principal, there is a different unloading curve for each S_0. In practice, because the right-hand side of Eq. 85 is independent of t, there is a single universal unloading curve. Thus we solve Eq. 85 with $S_0 = 1$ to get the unloading curve. This is easily done with a fourth-order Runge-Kutta method, in conjunction with an approximate analytical integration to move away from the singular point $S = 1$. Fig. 4 shows the result for $S(t)$. Various unloading times may be determined from this curve. For example, we see that it takes ~0.07 s to go from fully saturated to $S = 0.2$. As another example, consider the time required to go from an initial saturation of 0.8 to a saturation of 0.3. The time coordinates for these saturation values are, approximately, 0.01 and 0.05 s, so the time required is the difference, 0.04 s.

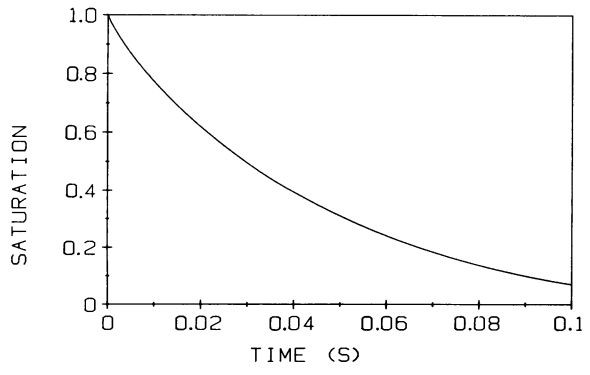

FIGURE 4 Mean red-cell oxygen saturation as a function of dimensional time for a red cell exposed to a zero oxygen tension. The time required to go from an initial saturation of S_A to a saturation of S_B is $t_B - t_A$, where t_A and t_B are the time coordinates corresponding to S_A and S_B on the graph.

Actual unloading times in vivo will be longer, because the red cell normally sees an oxygen tension much higher than zero in the capillary. Nevertheless, the lower bounds calculated here have their uses. For example, efficiency in oxygen transport requires that capillary transit times, even in extreme exercise states, exceed these lower bounds. Specifically, suppose red cells enter a capillary with a saturation of 0.8. In order to remove at least half of the available oxygen in the red cell, the transit time must exceed the time required to go from $S = 0.8$ to $S = 0.4$, which, from the graph, is 0.03 s.

SUMMARY

The asymptotic analysis has led to a simple picture of the state of an unloading red cell. In the interior of the red cell, oxygen and hemoglobin are essentially in chemical equilibrium. Near the red-cell membrane, there is a boundary layer in which deviations from chemical equilibrium occur. The transport resistance in this boundary layer is a major part of the total internal resistance of the red cell. Because of this, the oxygen gradients in an unloading red cell are small, except in the boundary layer. A helpful thermal analogue is the case of a warm metallic conductor, with a thin layer of insulation on its surface, immersed in a cold fluid.

Major mathematical simplifications are associated with the above picture. The systematic application of asymptotic methods has produced a simple lumped-parameter description of the unloading red cell. In effect, the two coupled, nonlinear, second-order partial differential equations are replaced by a single first-order ordinary differential equation for the mean saturation in the cell. By way of example, we have used the theory to calculate lower bounds on oxygen unloading times. This was done by analyzing the unloading process for a red cell in an environment of maximum demand, namely, zero oxygen tension on the cell boundary. A typical result is a time of ~0.05 for a cell to go from 90% saturation to 30% saturation.

The lumped parameter description derived here applies to cells of arbitrary shape. Thus it should be a useful tool in the modeling of the in vivo unloading process, a subject for future work.

We thank Professor Carl Honig, both for his frequent encouragement and for many helpful discussions. We thank Professor John Thomas for his helpful comments on the manuscript.

We are grateful for financial support from the National Institutes of Health, under grant number HL-18208.

Received for publication 30 January 1984 and in final form 23 August 1984.

REFERENCES

Baxley, P. T., and J. D. Hellums. 1983. A simple model for simulation of oxygen transport in the microcirculation. *Ann. Biomed. Eng.* 11:401–416.

Evans, E. A., and Y. C. Fung. 1972. Improved measurements of the erythrocyte geometry. *Microvas. Res.* 4:335–347.

Federspiel, W. J. 1983. Engineering analysis of two blood transport problems, Ph.D. thesis, University of Rochester, Rochester, NY. 326 pp.

Gibson, Q. H., F. Kreuzer, E. Meda, and F. J. W. Roughton. 1955. The kinetics of human hemoglobin in solution and in the red cell at 37°C. *J. Physiol. (Lond.).* 129:65–85.

Gijsbers, G. H., and H. J. van Ouwerkerk. 1976. Boundary layer resistance of steady-state oxygen diffusion facilitated by a four-step chemical reaction with hemoglobin in solution. *Pfluegers Arch. Eur. J. Physiol.* 365:231–241.

Hellums, J. D. 1977. The resistance to oxygen transport in the capillaries relative to that in the surrounding tissue. *Microvas. Res.* 13:131–136.

Himmelblau, D. M. 1964. Diffusion of dissolved gases in liquids. *Chem. Rev.* 64:527–550.

Honig, C. R. 1981. Modern Cardiovascular Physiology. Little, Brown & Co., Boston. 347 pp.

Huxley, V. H., and H. Kutchai. 1983. Effect of diffusion boundary layers on the initial uptake of O_2 by red cells. Theory versus experiment. *Microvas. Res.* 26:89–107.

Keller, K. H., E. R. Canales, and S. I. Yum. 1971. Tracer and Mutual Diffusion Coefficients of Proteins. *J. Phys. Chem.* 75:379–387.

Keller, K. H., and S. K. Friedlander. 1966. The steady-state transport of oxygen through hemoglobin solutions. *J. Gen. Physiol.* 49:663–679.

Kreuzer, F., and L. J. C. Hoofd. 1970. Facilitated diffusion of oxygen in the presence of hemoglobin. *Respir. Physiol.* 8:280–302.

Kreuzer, F., and L. J. C. Hoofd. 1972. Factors influencing facilitated diffusion of oxygen in the presence of hemoglobin and myoglobin. *Respir. Physiol.* 15:104–124.

Kutchai, H. 1970. Numerical study of oxygen uptake by layers of hemoglobin solution. *Respir. Physiol.* 10:273–284.

Linke, W. F. 1965. Solubilities, Vol. II. American Chemical Society, Washington, DC. Fourth ed. 1914 pp.

Moll, W. 1969. The Influence of Hemoglobin Diffusion on Oxygen Uptake and Release by Red Cells. *Respir. Physiol.* 6:1–15.

Sheth, B. V. 1979. Oxygen transport in hemoglobin solutions. Applications in the microcirculation. Master's thesis, Rice University, Houston, TX.

Sheth, B. V., and J. D. Hellums. 1980. Transient oxygen transport in hemoglobin layers under conditions of the microcirculation. *Ann. Biomed. Eng.* 8:183–196. 112 pp.

Spaan, J. A. E., F. Kreuzer, and F. K. van Wely. 1980. Diffusion coefficients of oxygen and hemoglobin as obtained simultaneously from photometric determination of the oxygenation of layers of hemoglobin solutions. *Pfluegers Arch. Eur. J. Physiol.* 384:241–251.

Van Dyke, M. 1975. Perturbation Methods in Fluid Mechanics. Parabolic Press, Stanford. Annotated ed. 271 pp.

Wintrobe, M. W., G. R. Lee, D. R. Boggs, T. C. Bithells, J. Foerster, J. W. Athens, and J. N. Lukens. 1981. Clinical Hematology. Lea & Febiger, Philadelphia. Eighth ed. 2021 pp.

Wittenberg, J. B. 1970. Myoglobin-facilitated oxygen diffusion. Role of myoglobin in oxygen entry into muscle. *Physiol. Rev.* 50:559–636.